

Electromagnetic and electrical co-simulation of the HERA analogue system with CST – Delay spectrum response and sensitivity calculation

Nicolas Fagnoni ⁽¹⁾, Eloy De Lera Acedo ⁽¹⁾, Christos Kolitsidas ⁽²⁾

⁽¹⁾ University of Cambridge, UK, Department of Physics

⁽²⁾ KTH Royal Institute of Technology, Stockholm, Sweden, Department of Electromagnetic Engineering

25th May 2017

Abstract

This memo presents a global electromagnetic and electrical co-simulation of the HERA analogue signal chain, combining the effects of the antenna with the RF front-end, which consists of an active balun connected to a receiver via coaxial cables. The circuits of the front-end are simulated with Genesys ¹, in order to obtain their S-parameters and noise figures. These results are then validated thanks to measurements performed with a VNA. From the noise figures, the system noise temperature and the antenna sensitivity can be calculated. Lastly, the S-parameters of the front-end are combined with the electromagnetic model of the antenna in CST. This co-simulation is excited by a plane wave, which allows us to obtain the output signal after the front-end in the time domain.

Introduction

In our previous memo ², we presented a detailed electromagnetic simulation of the HERA antenna performed with CST, and validated by measurements on a real dish built at Lord's Bridge (UK). Thus, it was possible to simulate the main parameters of the antenna, such as the radiation pattern, impedance, radiation and aperture efficiency, reflection coefficients, or its response to an incoming plane wave in the time and frequency domains.

However, in this model an arbitrary differential impedance of 100 Ω terminated the feed. Therefore the interactions with the RF front-end connected to the antenna were not properly taken into account. This is problematic because the impedance matching between the feed and the front-end can also have a strong impact on the received signal, and contribute to the chromatic effects induced by the system. In particular, there is an impedance discontinuity at the interface between the antenna output and the front-end input. Because of that, a part of the incoming signal is reflected back at this interface, then re-radiated by the dipoles, and reflected again by the parabola towards the feed, which creates additional ripples the time domain. So in order to improve our previous model, we have developed a simulation of the RF front-end, validated by measurements.

In the first section of this memo, the details of this new model are presented. For each element of the RF front-end, the S-parameters and the noise figure are simulated and measured. The S-parameters allow us to obtain information about the properties of reflection, transmission, attenuation, gain, and impedance for each block. Moreover, the system noise temperature can be calculated. As explained in the second section, the system noise temperature has a direct impact on the antenna sensitivity, and also depends on the input impedance connected to the RF front-end. Therefore, it is necessary to combine the noise simulation with the simulated or measured differential antenna impedance. Lastly in the third section, the S-parameters of the front-end and of the electromagnetic model of the antenna are associated in a co-simulation using CST. The system is then excited by a plane wave, and the time signal at the output of the front end is simulated. In particular, the effects of the amplification of the signal by the active balun and the receiver, along with its propagation in the cable, are visible. Thus, this approach allows us to update the results obtained in previous simulations ^{3,4}, with a more accurate model.

1. Analogue signal chain simulation

1.1. Model

So far HERA is still using the receiving system developed for PAPER by the NRAO, which consists of an active balun with pre-amplification stages, transmission coaxial cables, and a receiver board⁵⁶⁷ (see *Figure 1*). The different elements of the front-end as well as their main characteristics are represented in *Figure 2* by a block diagram, for a single polarisation.

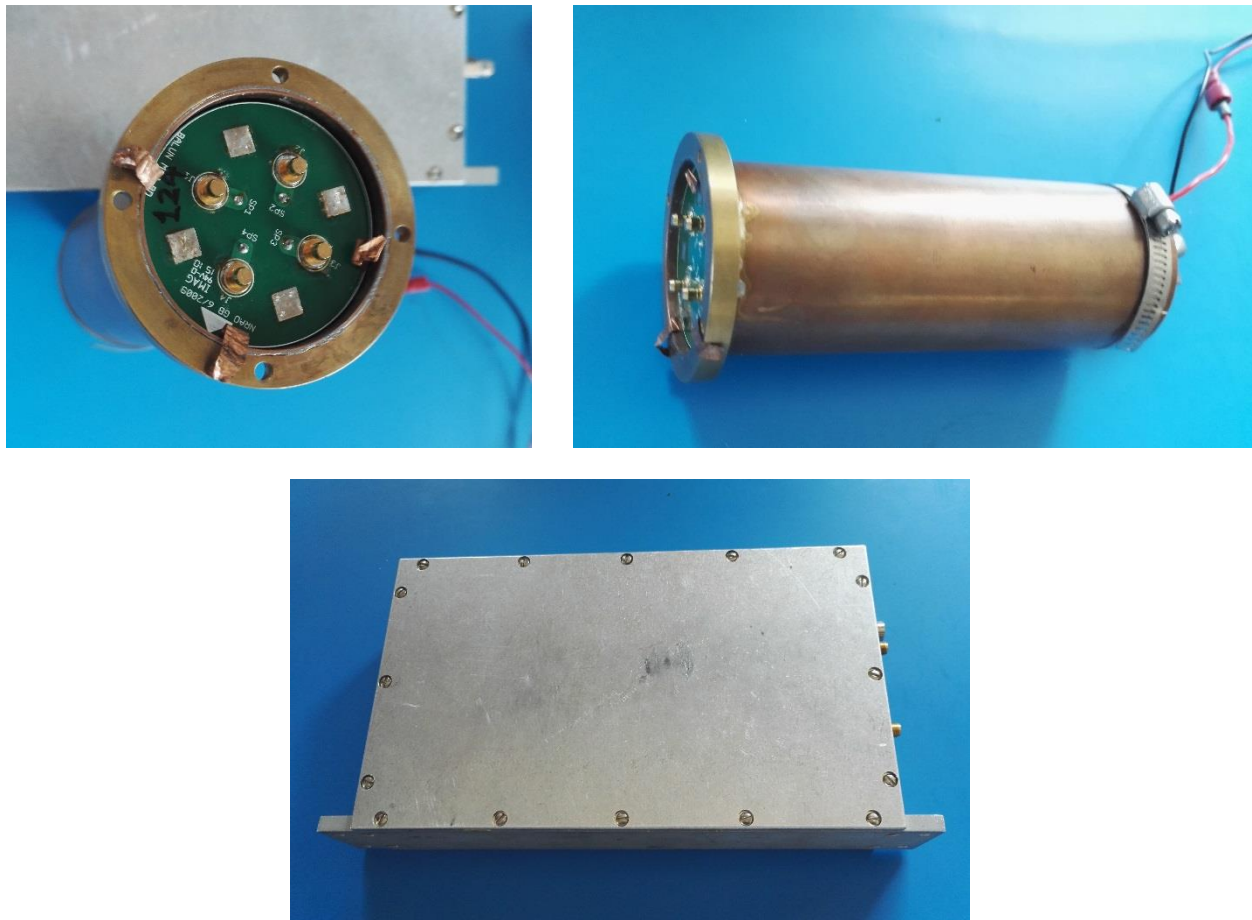


Figure 1. Pictures of the active balun (top) and receiver (bottom). These two elements are connected by RG6U twin coaxial cables.

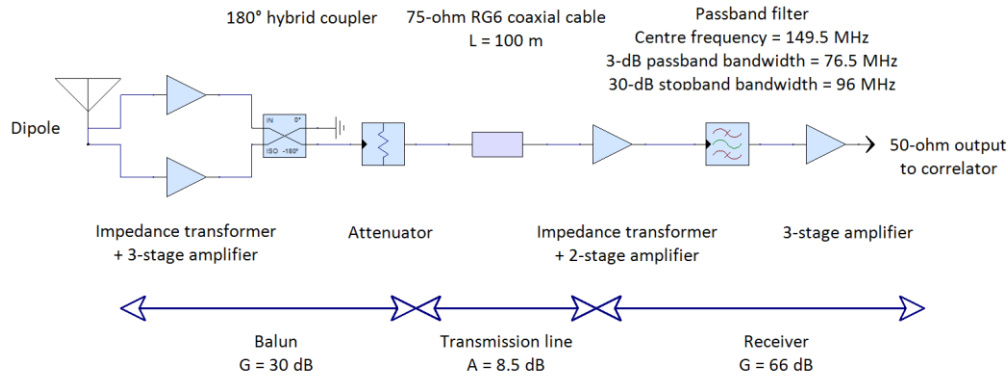


Figure 2. Block diagram of the RF front-end.

Each dipole arm is terminated by a feed bar, directly connected to an electrical input of the balun. Then, the antenna impedance is transformed using a three-winding transformer, and the signal is amplified by a cascade of two transistors plus one amplifier. A 180° hybrid coupler combines the two 180° out of phase signals coming from the dipole arms, and the unbalanced output signal is then transmitted to the receiver via a RG6U coaxial cable with an impedance of $75\ \Omega$ and terminated by F-connectors. Note that the impedance of the input ports of the 180° hybrid coupler is $50\ \Omega$, and that the impedance of the output port is $75\ \Omega$, in order to get a good impedance matching between the $50\text{-}\Omega$ output of the amplifier and the $75\text{-}\Omega$ input of the RG6U cable. Moreover, the balun is terminated by a 2.6-dB attenuator with a reverse isolation of 13.8 dB in order to limit the amplitude of the reflections between the balun output, the cable and the receiver. Thus, the global gain of the active balun is about 30 dB between 100 and 200 MHz (see Figure 3).

In our simulation and measurements, a 100-m RG6U twin coaxial cable is used to connect the balun to the receiver, which adds an attenuation between 6.5 and 9.5 dB as shown in Figure 4. Besides, the receiver is optimised to work with an impedance of $50\ \Omega$, and so the impedance matching with the $75\text{-}\Omega$ coaxial cable is also performed with a transformer. The receiver consists of a cascade of one transistor and four amplifiers separated by 3-dB attenuators for interstage isolation, which gives an additional gain of 66 dB (see Figure 5). Thus, in total the gain of the global chain is about 87.5 dB (see Figure 6). The receiver also includes a bandpass filter, with a 3-dB passband bandwidth of 76.5 MHz, centred on 149.5 MHz, and a 30-dB stopband bandwidth of 96 MHz. In our simulation, it is modelled by an elliptic filter with a very sharp roll-off to reproduce the filter response. Lastly, the output of the receiver is connected to the correlator with a $50\text{-}\Omega$ SMA cable. The active balun, coaxial cable and receiver were carefully simulated with the software Genesys, thanks to the provided electrical schematics. The components were modelled using the Genesys library and the data provided by the manufacturers^{8 9 10 11 12}.

The goal of this circuit simulation is to have a flexible tool to generate the S-parameters of the different elements of the front-end, in order to characterise these sub-systems in terms of reflected and transmitted power at their interfaces. Moreover, this simulation also allows us to estimate the noise added by the receiving system, and thus better quantify its impact on the array sensitivity.

1.2. Measurements and simulation of the signal chain characteristics

1.2.1. S-parameters

The forward gain (S_{21}), input and output reflection coefficients (S_{11} and S_{22}), and reverse gain (S_{12}) of the different sub-systems (active balun, coaxial cables and receiver), along with the global RF front end are simulated with Genesys, and then measured with a 4-port VNA. All the measurements were performed with a reference termination impedance of 50Ω , and the effects of the measurement cables were calibrated and automatically corrected.

It is also important to mention that in order to connect the SMA measurement cables of the VNA to the two input pin connectors of the balun, a small “adapter board” was inserted. Indeed, by definition the balun is a 3-port network which transforms the differential input signals received from the dipole arms into an unbalanced signal. In this configuration, the VNA measures the “single-ended” S-parameters associated to each of the 3 ports. However, since the balun responds to a balanced signal, it is preferable to describe its performance using the “mixed-mode” S-parameters, and in particular the “differential” S-parameters. In this case, the 2 input ports fed by the differential signals can be represented by only 1 global port. Thus, if the 2 balanced ports are numbered 1 and 2, and the unbalanced port 3, the differential S-parameters are given by the following formulas^{13 14}:

$$S_{3d} = \frac{S_{31} - S_{32}}{\sqrt{2}} \quad (1), \text{ the transmission parameter between the differential port and the unbalanced port}$$

$$S_{d3} = \frac{S_{13} - S_{23}}{\sqrt{2}} \quad (2), \text{ the transmission parameter between the unbalanced port and the differential port}$$

$$S_{dd} = \frac{S_{11} - S_{12} - S_{21} + S_{22}}{2} \quad (3), \text{ the reflection parameter of the differential port}$$

S_{33} , the reflection parameter of the unbalanced port

The S-parameter measurements of the cable and receiver is rather straightforward, since these are 2-port networks. However, one of the main difficulties is the fact that the amplifier chain in the active balun or in the receiver provides a very high gain, and so can very quickly saturate, which affects the reliability of the measurements. Therefore, we have to be careful with the level of input power applied. Thus, an input power of -70 dBm was used with the receiver, and -45 dBm with the balun. Nevertheless, in this case the measurements can be a little bit noisy, and so must be “averaged”.

The figures below show the S-parameters from our simulations and measurements. As we can see, we managed to create a rather reliable model of the RF front-end.

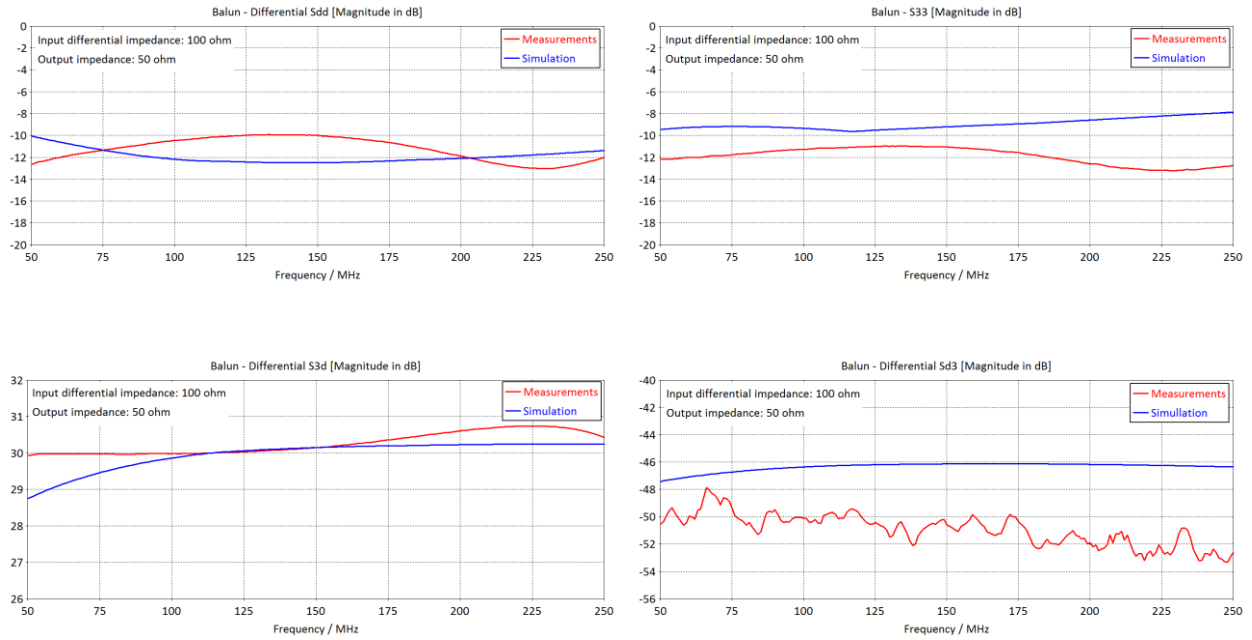


Figure 3. S-parameters of the active balun, with respect to an input differential impedance of 100 Ω , and output single-ended impedance of 50 Ω .

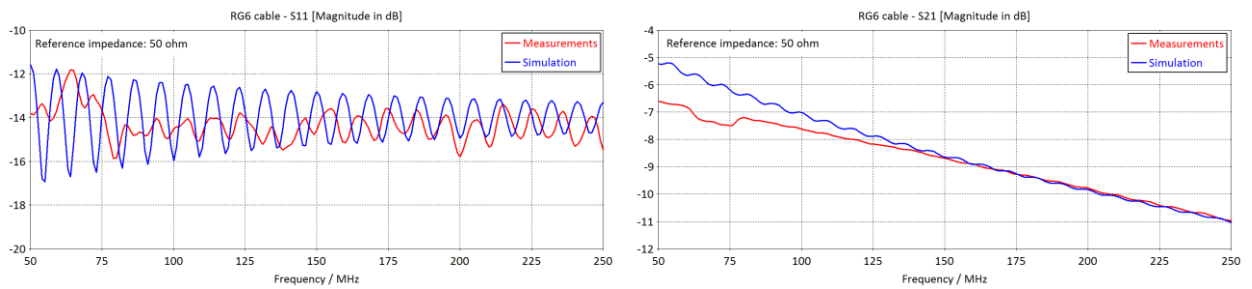


Figure 4. S-parameters of the RG6U coaxial cable (100 m), with respect to 50 Ω .

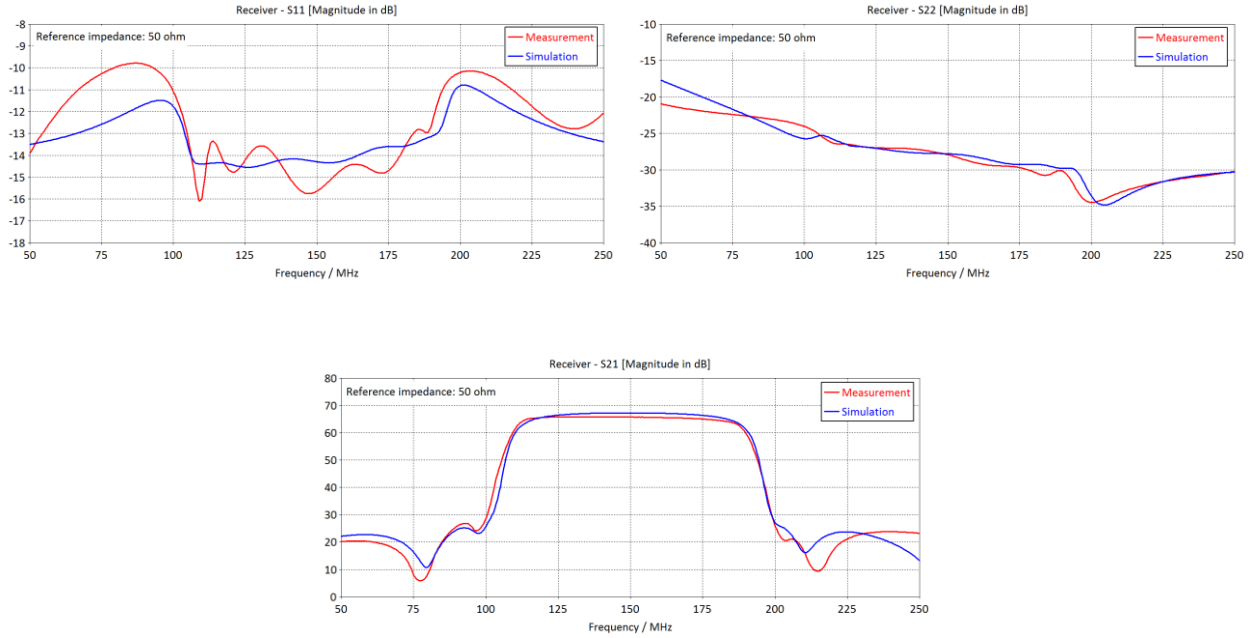


Figure 5. S-parameters of the receiver, with respect to 50 Ω . The reverse gain S_{12} is extremely low (< -120 dB in simulation) and its measurements is actually limited by the noise floor of the VNA (about -90 dB)

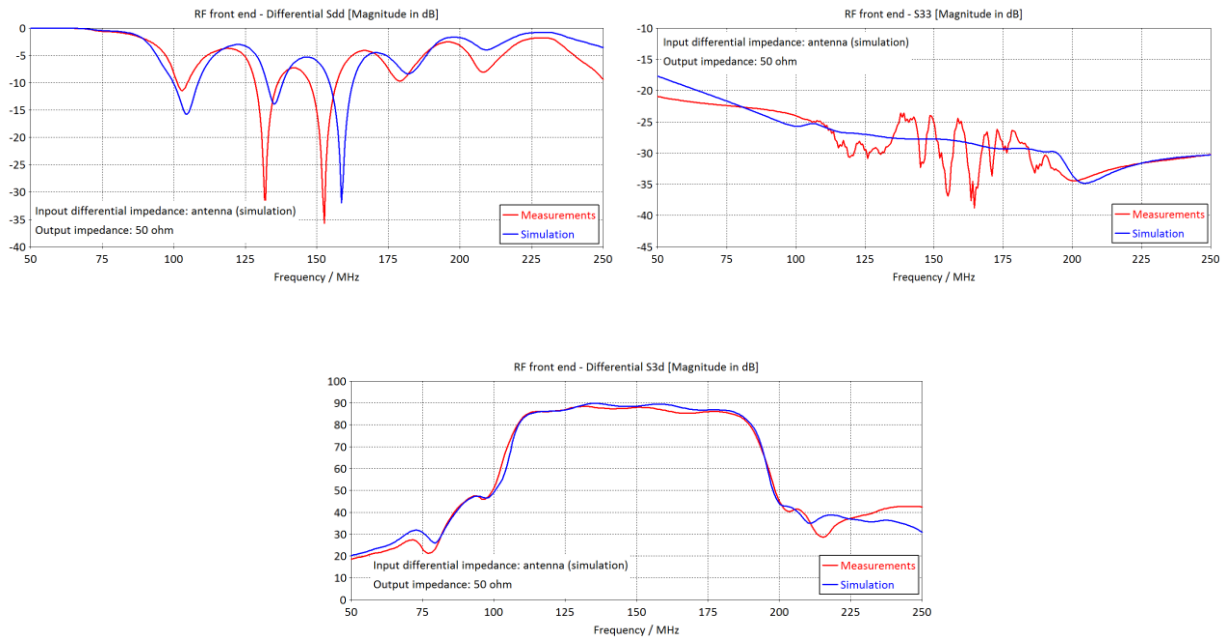


Figure 6. S-parameters of the global RF front-end, using the simulated antenna impedance as differential input impedance and 50 Ω as output impedance.

1.2.2. Termination impedance

The Z-matrix of the different components can be obtained from their S-parameters, and their input impedance Z_{in} calculated. Thus, for a 2-port network ¹⁵:

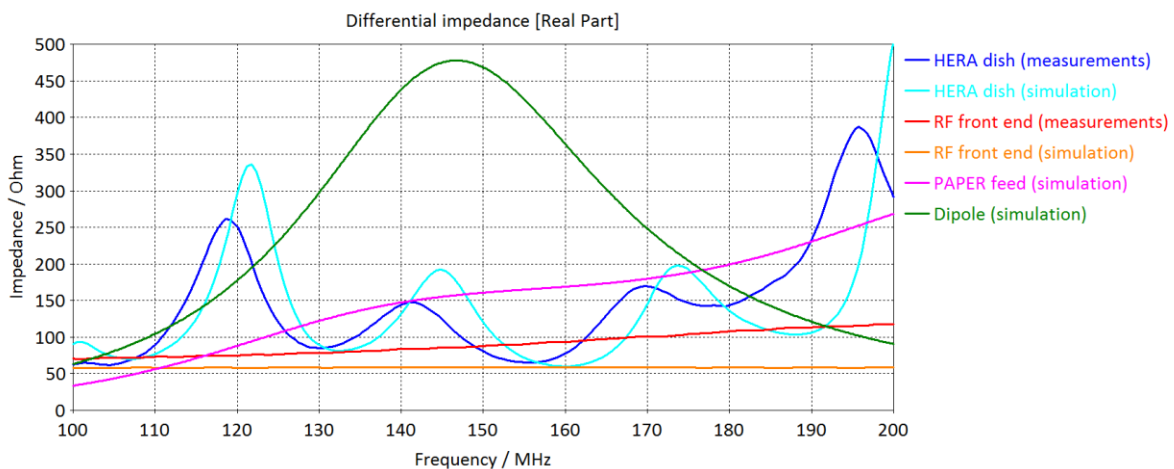
$$Z_{in} = Z_{11} - \frac{Z_{12}Z_{21}}{Z_{22} + Z_L} \quad (4)$$

with Z_L the load impedance connected to the output port 2, typically 50 Ω . Note that in the case of a 3-port network defined by a balanced input port, the differential Z-matrix is used to obtain the differential input impedance.

In particular, it is interesting to compare the differential input impedance of the HERA dish with the RF front end (see *Figure 7*). We can notice that there is a large disparity, which causes a problem of impedance mismatch. Thus, a part of the received power is reflected at the interface between the antenna and the RF front-end. Besides, when comparing the input impedance of the active balun and of the RF front end, it appears that they are very similar, which actually means that the mismatch mainly occurs at the interface with the balun, and that the rest of the chain is rather well matched.

In order to limit this problem and maximise the power transmitted to the front-end, ideally the impedance of the antenna should be equal to the complex conjugate of the impedance of the front-end, but in practice, this is something very complicated to achieve since the real and imaginary parts of the HERA dish impedance fluctuates a lot. On the other hand, we can also notice that the impedance of the PAPER feed, i.e. the dipole surrounded by the metal plates but without the backplane and the skirt, is rather smooth and not far from the impedance of the balun. This does illustrate the fact that the front-end was optimised for PAPER. Note that this is confirmed by *Figure 20* which shows that the differential S-parameter of the PAPER dipole terminated by the front-end is rather low and stable. Lastly, by looking at the impedance of a simple dipole and the one of the PAPER feed, we can clearly see the benefits of adding the metal plates around the dipoles; the feed impedance is much flatter.

Thus, this analysis illustrates the impact of the addition of the parabola on the antenna impedance, and why it is a challenging task to match its impedance.



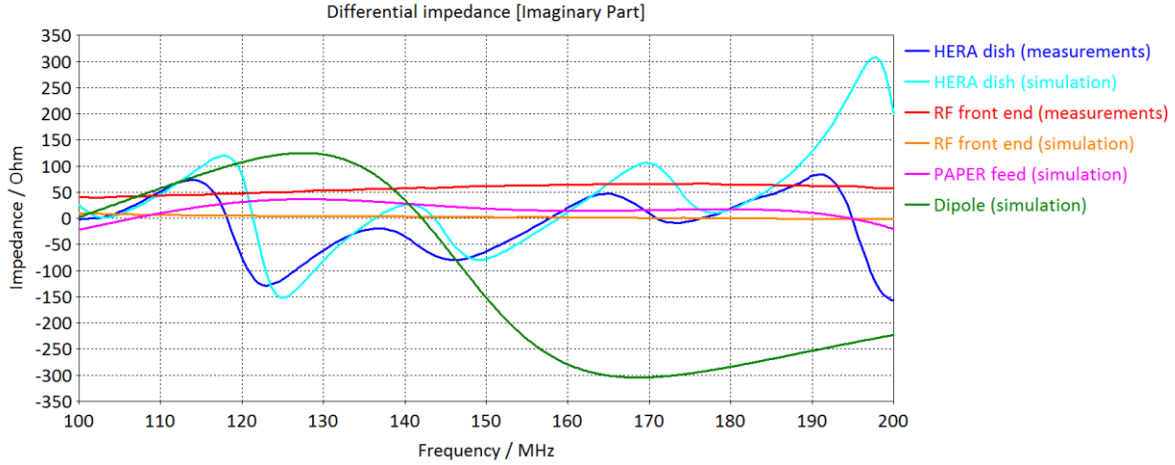


Figure 7. Real and imaginary parts of the differential input impedance of the RF front end and antenna, from measurements and simulations.

1.2.3. Noise figure

In order to precisely characterise the effects of the RF front-end on the received signal, it is also essential to consider the noise from the electrical components, such as thermal noise generated by all the components with a certain internal resistance, or shot noise produced by the bipolar transistors and amplifiers. Indeed, the RF front-end noise directly affects the sensitivity of the antenna as explained in the next section.

As previously, the noise figure of each elements was measured and then simulated with Genesys. In the case of the active balun, it is important to specify that a passive 180° power splitter was added on the adapter board. Thus, the input power from the VNA measurement port is equally divided between the 2 balanced input ports, and so the system can be considered as a 2-port network. In this case, the differential noise figure is actually measured, but on condition that the contribution from the splitter is de-embedded. To do so, first the single-ended S-parameters of the 3-port splitter must be measured with the VNA (input ports numbered 1 and 2, output port numbered 3). Then, one can demonstrate using the Friis formula (see Equation 7) that the measured global noise factor F_{cas} of the splitter plus the active balun is equal to ¹⁶:

$$F_{cas} = \frac{1}{2} F_{spl} + \frac{F_{bal} - 2}{4G_{spl}} \quad (5)$$

with F_{spl} the single-ended noise factor of the splitter, F_{bal} the single-ended noise factor of the balun, and G_{spl} the single-ended “gain” of the splitter. However, since the splitter is a passive device, its single-ended noise figure is directly equal to its attenuation. Thus:

$$F_{spl} = \frac{1}{G_{spl}} = \frac{1}{|S_{spl\ 13}|^2} \quad (6)$$

Then, F_{bal} can be calculated. However, it corresponds to the single-ended noise factor between one of the balanced input port and the unbalanced output port. In order to obtain the differential noise factor, this value must be simply divided by 2. Note that this formula assumes that the VNA, splitter, and balun are properly matched, that the splitter and balun are “symmetric”, and that the balanced ports are perfectly isolated ($S_{12} = S_{21} = 0$). Lastly, it should be made clear that the noise figure is actually the noise factor but expressed in dB.

As previously mentioned, the noise factor of the cable can be deduced from its S-parameters. Concerning the receiver, the noise measurement is straightforward on condition that the amplifiers are not saturated. The comparative results are given below, with respect to a termination impedance of 50 Ω , or a differential termination impedance of 100 Ω for the balun.

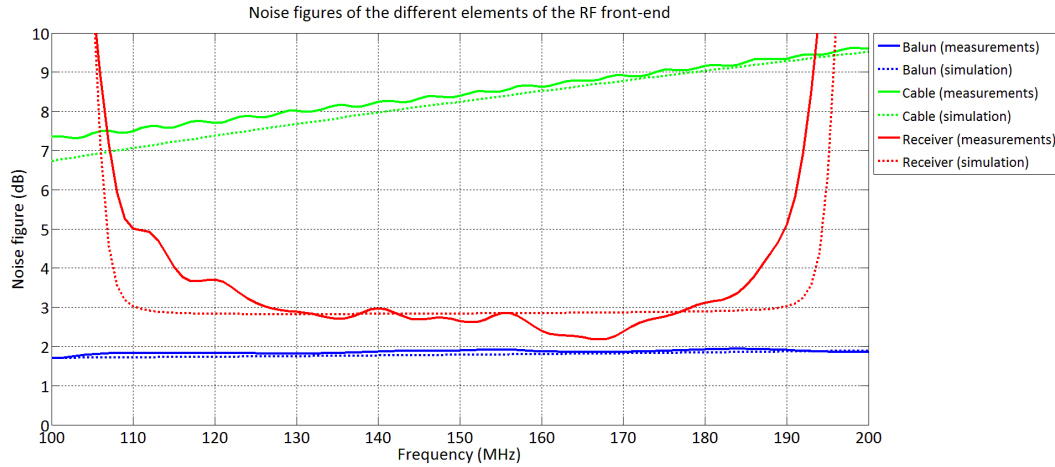


Figure 8. Noise figure of the active balun, cable, and receiver, from measurements and simulation.

Then, by using the Friis formula (see Equation 7), it is possible to estimate the noise factor F_{RF} of the front-end. As expected, it is very close to the noise factor of the first block, i.e. the active balun (see Figure 9). Besides, the level of noise generated can also be expressed in terms of noise temperature at a reference temperature T_0 of 290 K (see Equation 8 and Figure 12).

$$F_{RF} = F_{bal} + \frac{F_{cab} - 1}{G_{bal}} + \frac{F_{rec} - 1}{G_{bal}G_{cab}} \quad (7)$$

$$T_{RF} = T_0 (F_{RF} - 1) \quad (8)$$

Lastly, there is another essential parameter to consider: the input impedance of the RF front-end. Indeed, as shown by Equation 9¹⁷, the noise factor of an amplifier F_{amp} depends on the source impedance at its input.

$$F_{amp} = F_{min} + \frac{R_N}{R_S} |Y_S - Y_{opt}|^2 \quad (9)$$

with F_{min} the minimum noise factor of the amplifier, R_N its equivalent noise resistance, Y_{opt} the optimum source admittance which minimises the noise factor, Y_S the source admittance (i.e. the antenna) and R_S its real part. Our simulation also allows us to obtain these parameters. They depend on the frequency, but fortunately they do not vary a lot between 100 and 200 MHz. Thus, in the case of the active balun, F_{min} varies between 1.6 dB and 1.8 dB, $Z_{opt} = 1/Y_{opt}$ between 119 + 34i Ω and 148 + 22i Ω , and R_N is around 27 Ω .

In other words, the noise factor of the balun is different depending whether the differential source impedance is 100 Ω like in our measurements, or the antenna. Moreover, this equation shows that the noise generated by the front-end can be minimised on condition that it is connected to an optimal impedance. However, the input impedance required to minimise the generated noise is different from the impedance necessary to minimise the reflections between the antenna and the front-end. Thus, a trade-off has to be made. Nevertheless, the effects of

the receiver noise can be mitigated by increasing the integration time, whereas it is more complex to correct the systematics introduced by the reflections.

Since it is technically complicated to measure the noise factor of the balun connected to the antenna impedance, we have to rely on simulation. As we can see on *Figure 10*, the noise figures of the RF front-end obtained from measurements and simulations with a 100- Ω impedance agree well, and is around 1.8 dB, or 150 K in terms of noise temperature. Therefore, we can use our simulation to get a coherent estimate of the noise figure of the front-end when it is connected to the antenna. The effects of the filter bandwidth, combined with an important impedance mismatch for the noise at high frequency (see *Figure 7*), are clearly visible below 105 MHz and above 190 MHz: the noise figure rockets and it may be difficult to retrieve useful data for these frequencies. We can also notice the effects of the variation of the antenna impedance (measured or simulated) on the generated noise, which oscillates between 1.7 and 2.4 dB, namely between 140 and 215 K (see *Figure 12*).

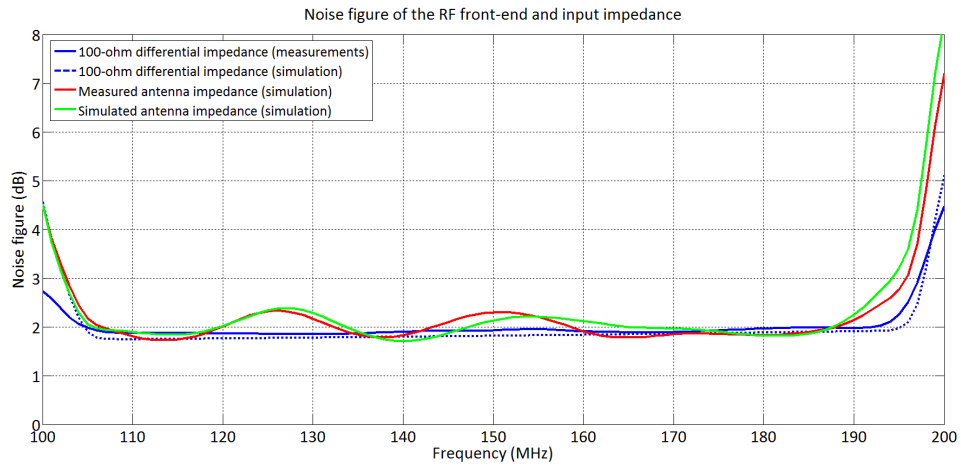


Figure 9. Calculated noise figure of the RF front-end, when it is connected to a differential impedance of 100 Ω , the measured and the simulated antenna impedance.

2. System temperature and antenna sensitivity

In this memo, we define the antenna sensitivity S_a at the feed point of the antenna for a single element, and for a given polarisation, as the ratio of the effective antenna aperture A_{eff} over the system noise temperature T_{sys} ^{18 19}. Thus, this figure of merit has the advantage to take into account the gain of the antenna along with the signal received, and the different sources of losses and noise.

$$S_a(\theta, \varphi) = \frac{A_{eff}(\theta, \varphi)}{T_{sys}} \quad (10)$$

The effective antenna aperture, which accounts for the fact that not all the physical surface of the antenna collects the signal with the same efficiency, is then defined by:

$$A_{eff}(\theta, \varphi) = \frac{\lambda^2}{4\pi} G(\theta, \varphi) \quad (11)$$

with λ the wavelength, and $G(\vartheta, \varphi)$ the antenna gain. Note that the antenna gain is equal to the ratio of the radiated power $P(\vartheta, \varphi)$ in a given direction defined by the angles ϑ and φ over the power accepted by the antenna from the feed line P_{acc} divided by 4π . In this definition of A_{eff} , the losses arising from polarization and impedance mismatches are not taken into account, but only the dissipative losses caused by the dielectric and metal elements of the antenna. It is also equal to the directivity $D(\vartheta, \varphi)$ times the antenna radiation efficiency η_{rad} :

$$G(\theta, \varphi) = \frac{P(\theta, \varphi)}{\frac{P_{acc}}{4\pi}} = D(\theta, \varphi) \eta_{rad} \quad (12)$$

The antenna gain, and so the effective antenna aperture, its radiation efficiency, and power radiation pattern, can be obtained via our CST simulation. The maximum effective antenna aperture represents about 70% of its physical aperture (see Figure 10), and only 2-3 % of the received power is dissipated by the metal and dielectric elements of the antenna (see Figure 11). Thus, the gain and directivity are quasi-equivalent, and so the radiation losses are negligible in this case.

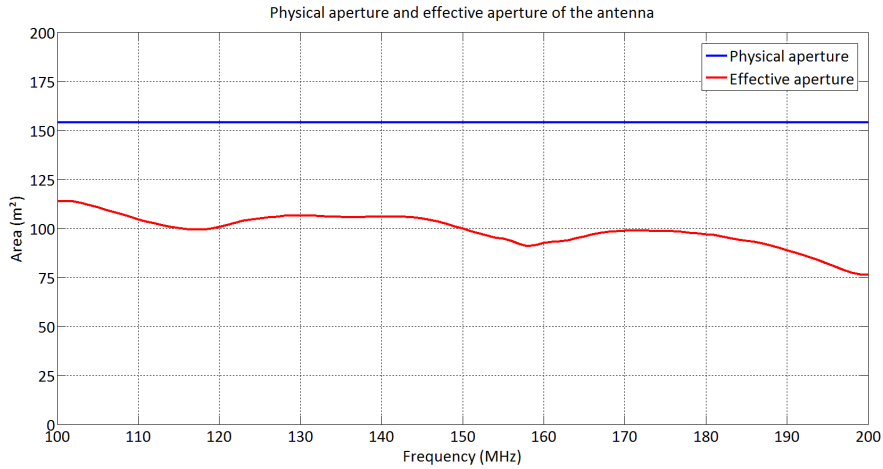


Figure 10. Physical antenna aperture and effective antenna aperture.

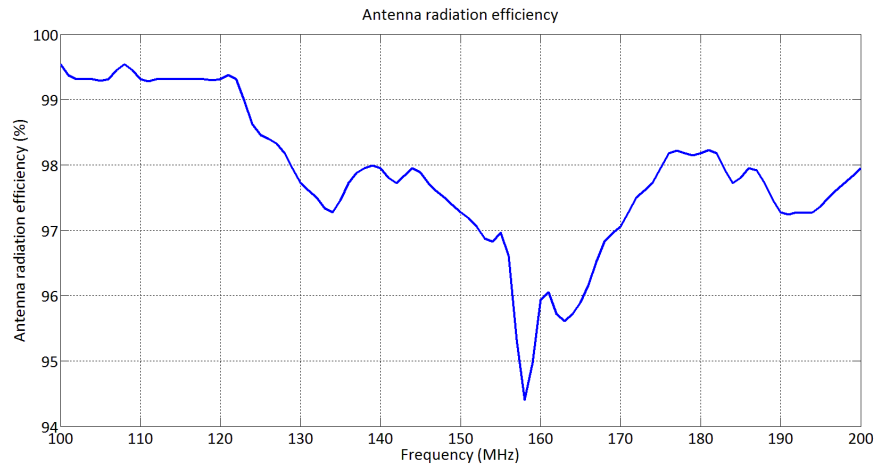


Figure 11. Antenna radiation efficiency.

The system noise temperature is the sum of all the noise contributions from the antenna T_{ant} and from the RF front-end T_{RF} . Note that in our simulation, T_{RF} does include the effects of the impedance mismatch with the antenna.

$$T_{sys} = T_{ant} + T_{RF} \quad (13)$$

Moreover, T_{ant} can be decomposed into two terms: a first term associated to the losses caused by the dissipative elements of the antenna at the ambient temperature $T_0 = 290$ K, and a second term corresponding to the noise effectively received by the antenna T_A , and coming from cosmic sources, but also from the atmosphere or the ground. Besides, the noise from cross-polarization leakage is neglected here, given the good isolation between the dipoles. Hence:

$$T_{ant} = T_0(1 - \eta_{rad}) + T_A \eta_{rad} \quad (14)$$

Lastly, the global noise temperature received by the antenna beam pointing at the zenith is given by:

$$T_A = \frac{\iint_{4\pi} T_b(v, \theta, \varphi) P_n(v, \theta, \varphi) \sin\theta \, d\theta \, d\varphi}{\iint_{4\pi} P_n(v, \theta, \varphi) \sin\theta \, d\theta \, d\varphi} \quad (15)$$

with T_b the brightness temperature distribution surrounding the antenna, and P_n its power radiation pattern. Now in order to simplify the model, the contribution from the atmosphere can be neglected at low frequency, as well as the emissions and scattering from the ground. Thus, in this case the received noise temperature is simply the “sky” temperature. In this memo, two different sky models are used.

First, a simple uniform sky, with a brightness temperature following a power law, is considered (see *Figure 12*). For a “cold” patch of the sky, typically observed by HERA far from the galactic centre and at low frequency, the sky temperature can be approximated by²⁰:

$$T_{sky} = 180 \left(\frac{\nu}{180 \text{ MHz}} \right)^{-2.6} \quad (16)$$

Figure 12 shows the different noise contributions in the system temperature. As expected, the sky temperature dominated by the galactic synchrotron emission is the main contribution, in particular at low frequency, but then decreases. On the other hand, as previously explained, the effects of the RF front-end are not negligible as the frequency increases.

By combining all these terms, the antenna sensitivity for a single element and a given polarisation, can be calculated, in particular by using the system temperatures obtained with the measured antenna impedance (see *Figure 13*). Since it is a function of the angles ϑ and φ , as an example the sensitivity for a signal with an angle of arrival of 0° (zenith), 5° , and 10° , and in the E-plane (the plane of the excited dipole) and in the H-plane (the plane perpendicular to the E-plane), is plotted. We can notice that the antenna is slightly more sensitive in the E-plane, which means that the beam is not perfectly circular, but tends to be wider in the plane of the considered dipole. In addition, in order to illustrate the effects of the input impedance, the noise temperatures and sensitivity are calculated when the RF front-end is connected to a differential impedance of $100 \, \Omega$ (data from measurements), and to the measured antenna impedance. The overall performance is slightly degraded when the antenna impedance is considered, mediocre below 105 MHz ($\sim 0.1 \text{ m}^2/\text{K}$), and bad after 195 MHz ($\sim 0.05 \text{ m}^2/\text{K}$).

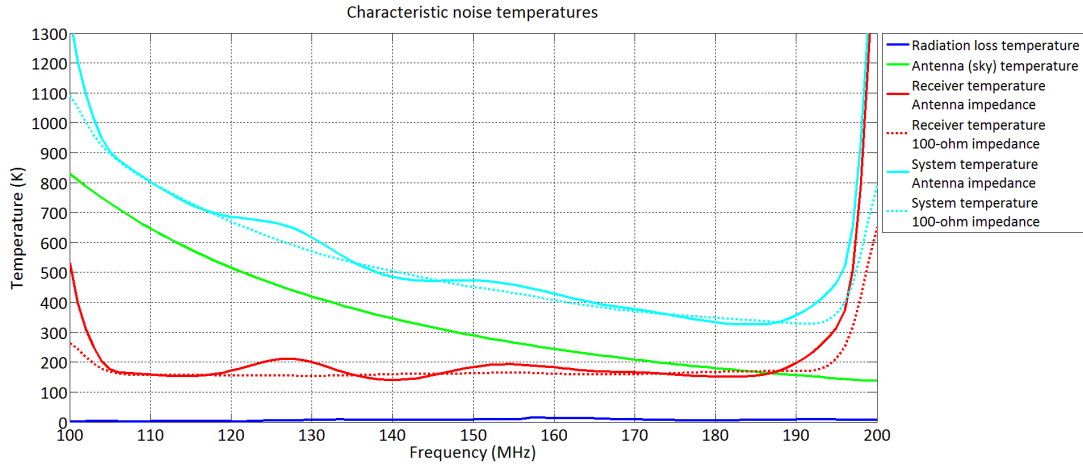


Figure 12. Noise contributions in the system noise temperature, for a differential input impedance of 100Ω , and for the measured antenna impedance. Uniform sky model.

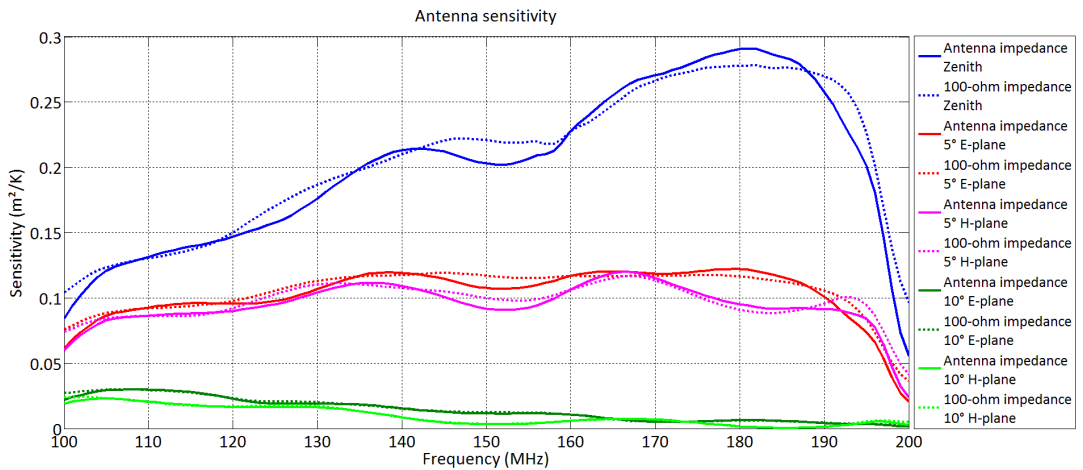


Figure 13. Antenna sensitivity for a single element, and at a zenith angle of 0° , 5° , and 10° , and in the E-plane and H-plane. Uniform sky model.

Lastly, in order to improve this model, a more sophisticated map of the sky temperature, the Haslam 408-MHz all-sky map extrapolated to lower frequencies²¹, was convolved with the antenna beam. This allows us to obtain a more realistic antenna temperature, which depends on the day, time, and location²². As an example, the antenna temperature received by a dish in the Karoo desert was simulated for the date of 20th July 2018, every 15 minutes for 24 hours, and between 50 and 250 MHz (see Figure 14). In particular, we can clearly see the effects of the galactic centre passing above the main beam between 19:00 and 22:00 UTC, which strongly impacts the sensitivity ratio. Nevertheless, for “quieter” areas, the temperature decreases from about 1 000 K at 100 MHz to 150 K at 200 MHz, which gives coherent results with our previous uniform sky model.

Thus, this is an important figure of merit to quantify and compare the performances of the system including the antenna along with its front-end, and the sky. Besides, using a realistic sky model will allow us to optimise the observation time of the telescope.

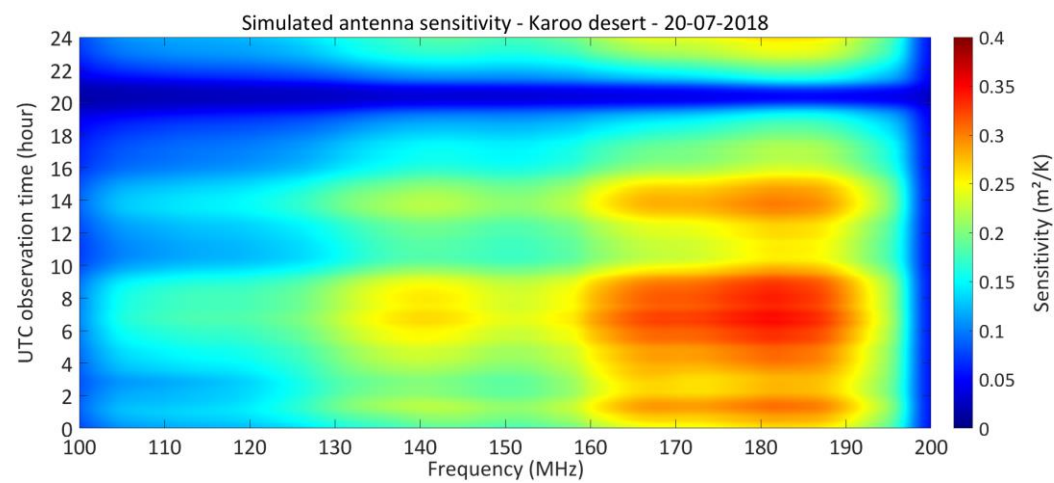
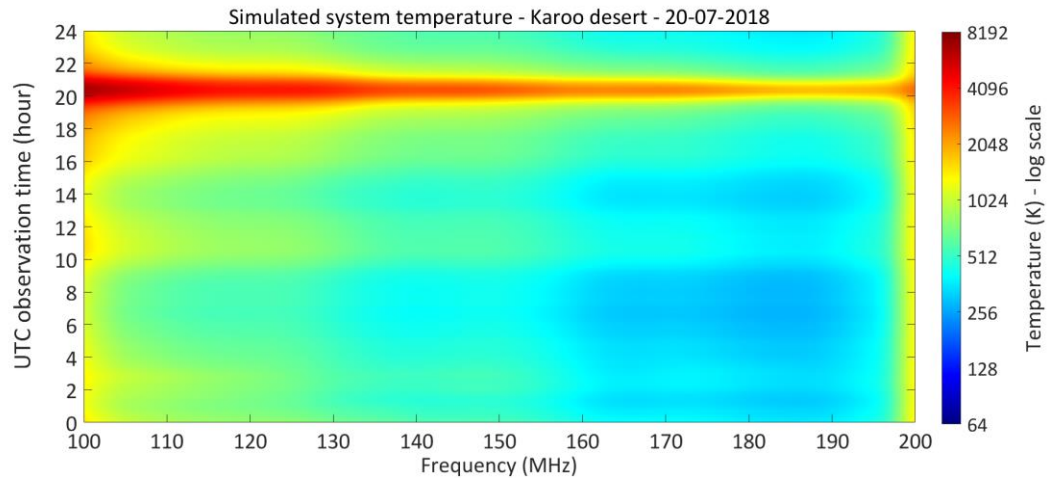
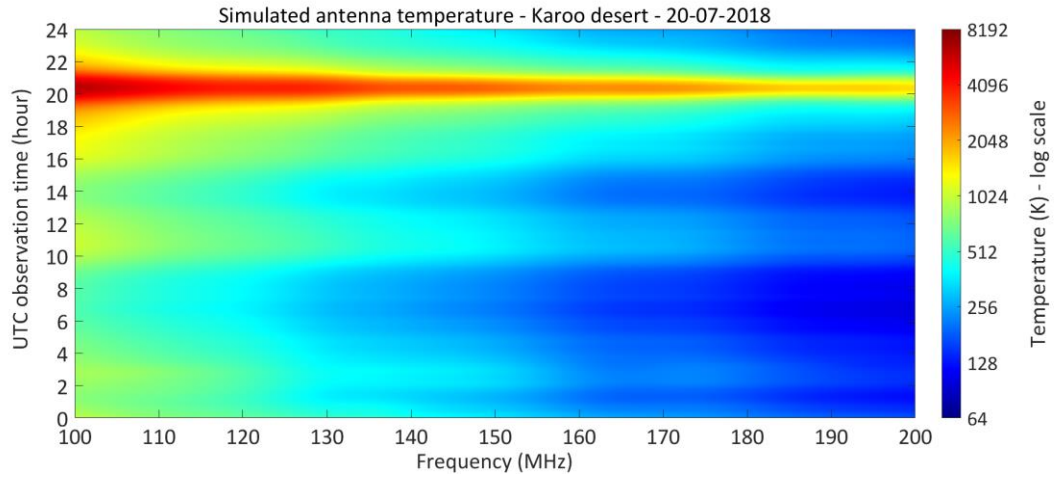


Figure 14. Simulated antenna temperature, system temperature, and antenna sensitivity at the zenith, in the Karoo desert, on 20th July 2018. Haslam sky model.

3. Electromagnetic and electrical co-simulation

3.1. Method

We have created a detailed simulation of the RF front-end which allows us to better understand its effects on the received signal, in terms of reflections and generated noise. By using CST, we have the possibility to combine the electromagnetic model of the antenna that we previously developed (c.f. HERA memo #21²), with the S-parameters of the RF front-end. Thus, instead of terminating the antenna by an arbitrary impedance in the simulation, for example $100\ \Omega$, we can use a more realistic approach by simulating the characteristics of the RF front-end, which depends on the frequency. This is important to better estimate the level of reflections which can contaminate the EoR window.

In CST Design Studio, the antenna electromagnetic model is cascaded with the S-parameters of the balun, coaxial cable, and receiver (see *Figure 15*), and the system is excited by an external plane wave coming from the zenith and linearly polarised. The transient solver is used, and the antenna response is simulated between 50 and 250 MHz, with a time step of about 0.004 ns and for 1000 ns, in order to be able to detect the multiple reflections occurring within the system up to the output of the front-end. The simulation uses an antenna model with 18.4 million cells, and takes about 7 h 45 min, using 2 CPU cores with a total of 16 parallel threads at 2.6 GHz, 29 GB of RAM, and without GPU acceleration.

Note that in CST, we must manually specify that the S-parameter blocks of the balun and receiver correspond to active components. Lastly, it is important to emphasise that the S-parameters of the front-end were simulated between 10 and 500 MHz. Indeed, this parameter does influence the time results: during the transient simulation, CST actually extrapolates these data in order to be able to combine them with the antenna response from the electromagnetic model. As we can see in *Figure 19*, even if we specify in CST that the signal has a bandwidth between 50 and 250 MHz, there is still a certain quantity of power outside this bandwidth. Consequently, in order to avoid extrapolation errors during the simulation, it is preferable to provide accurate data over a larger bandwidth.

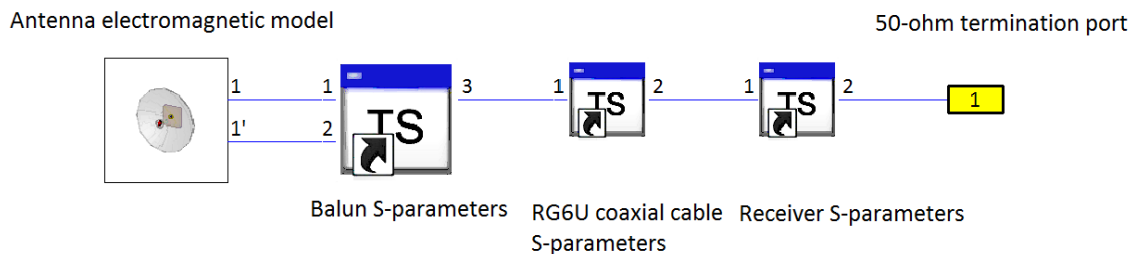


Figure 15. Block diagram of the co-simulation performed with CST, for a given polarisation.

3.2. Results

3.2.1. Time domain simulation and antenna response

As clearly developed in A. Ewall-Wice's paper³, the antenna can be considered as a "linear and time-invariant" system which can be described thanks to its transfer function or voltage response, in the time and frequency domain. In this approach, the antenna convolves (*) the received signal $in(t)$ with its voltage response $r(t)$, yielding the output signal $out(t)$. Since the input and output signals are known thanks to the co-simulation, it is then possible to estimate the antenna response. Mathematically, we have:

$$out(t) = in(t) * r(t) \quad (17)$$

so thanks to the convolution theorem, this equation can be transformed in the frequency domain. The antenna transfer function $R(f)$ is actually the ratio of the Fourier transform FT of the output signal over the Fourier transform of the input signal:

$$R(f) = \frac{FT[out(t)]}{FT[in(t)]} \quad (18)$$

Then, by taking the inverse Fourier transform, we can obtain the antenna response in the time domain.

Figure 16 shows the simulated voltages at different points of the analogue signal chain. Note that in this simulation, we considered cables with a length of 35 m, in order to illustrate the effects of the use of shorter cables on the delay power spectrum for a potential new design. The electromagnetic wave is emitted 5.4 m above the antenna (height of the simulation box), then is reflected by the parabola before reaching the feed at 4.9 m. Thus, the emitted signal has travelled for about 34 ns before reaching the dipole, generating the differential signals that we can observe. The active balun transforms the signals into an unbalanced signal and amplifies it by about 30 dB. Besides, once the main signal is received, we can also clearly see the reflections occurring at the interface between the balun and the antenna, which are then re-radiated by the dipole and reflected back by the parabola, every 33 ns (round trip time between the feed and the parabola). It is also interesting to see that the propagation and attenuation of the signal is also what we expect for a 35-m RG6U cable with a velocity factor VF of about 75 % ($VF = \frac{v}{c} = \frac{1}{\sqrt{\epsilon_r}}$) with $\epsilon_r = 1.78$, namely 156 ns and -3 dB. The signal reaching the receiver is then amplified by about 66 dB and shaped by the bandpass filter. Lastly, the simulation does show the presence of additional ripples about 312 ns after the main signal is received. This group of ripples is actually caused by the reflections which occur at the interfaces of the 35-m coaxial cable. Thus, this simulation is an interesting tool to model the chromatic effects induced by the antenna, along with the propagation and amplification of the signal in the RF front-end.

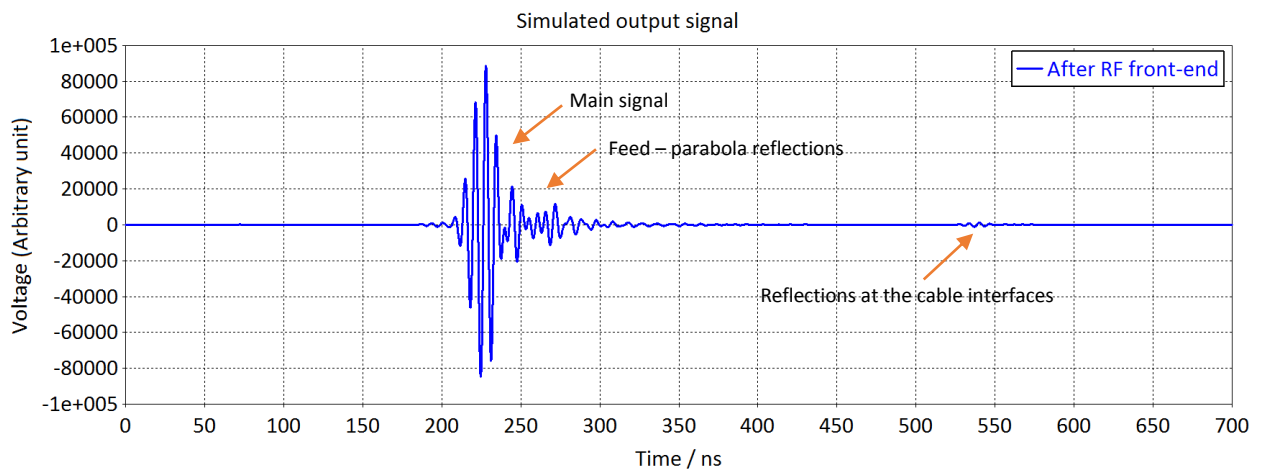
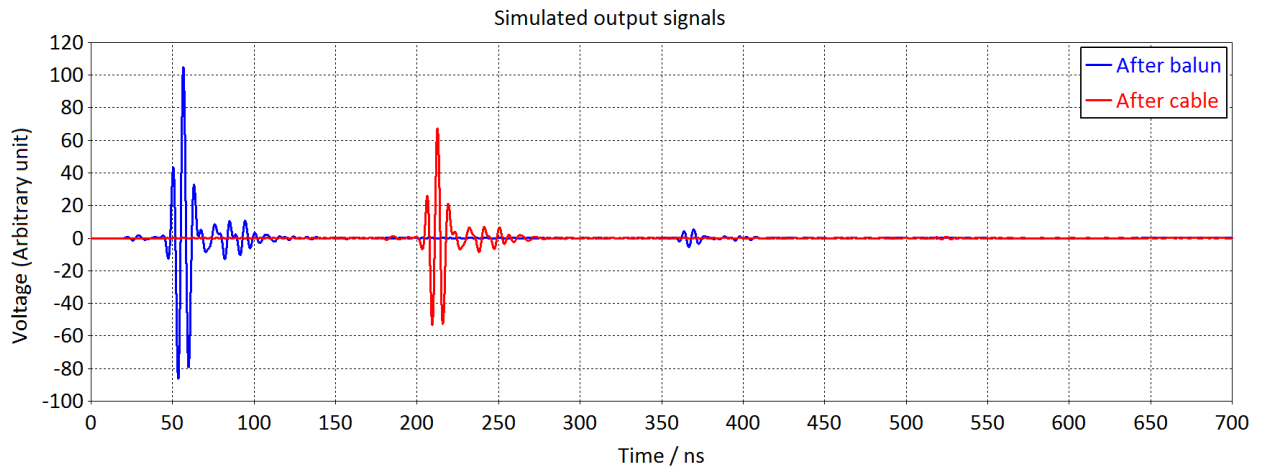
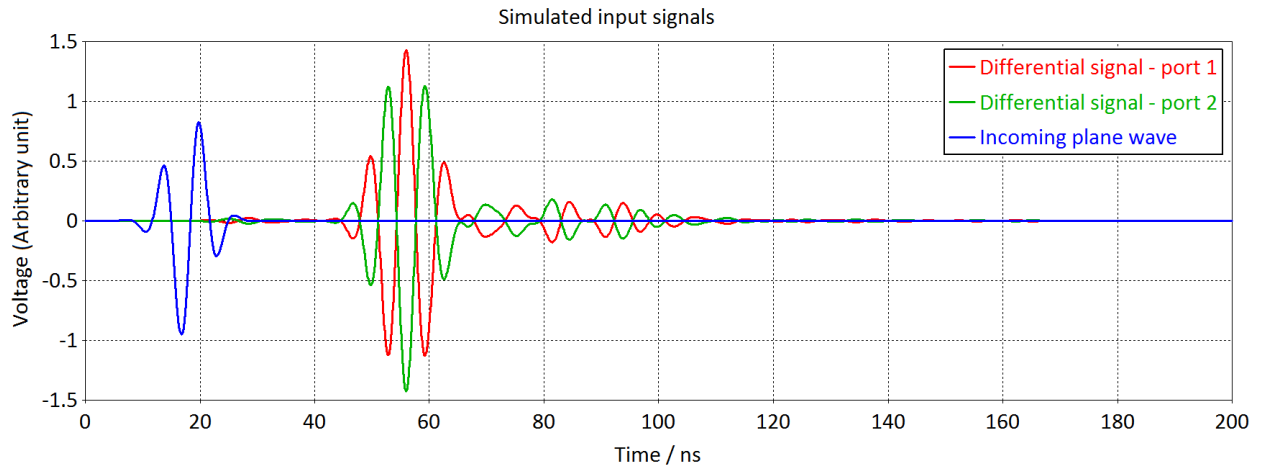


Figure 16. Simulated input signals and output signals, before and after the balun, after the 35-m cable, and at the end of the RF front-end. The voltage is in arbitrary unit. Component models from simulation.

As previously described, the voltage antenna response in the time domain can now be computed. Besides, in order to better illustrate the effects of the termination on the antenna response, we simulated the output signal with a fix differential impedance termination of 50, 100, and 200 Ω , and with the simulated and measured S-parameters of the RF front-end.

Moreover, in order to account for the fact that the correlator has a finite bandwidth between 100 and 200 MHz, the frequency transfer function $R(f)$ is multiplied by a window function $W(f)$ in the frequency domain. Note that this is equivalent to convolve the antenna response $r(t)$ by the inverse Fourier transform of the window in the time domain. This has the advantage to remove the noise which would affect the calculated time antenna response. Indeed, in our simulation, the input and output signals have a finite and compact frequency support, which tends to “zeros” after about 400 MHz (see Figure 19). Consequently, the amplitude of the ratio $R(f)$ greatly increases and becomes noisy, which affects the time response. As N. Thyagarajan showed ⁴, a Blackman-Harris window is a good choice. Indeed, the Fourier transform of a window function presents sidelobes which spread the signal, and so the foreground in the time domain. However, this specific window function has very low sidelobes, but the drawback is that it has a limited sensitivity, compared to a rectangular window for example.

Lastly, in order to estimate and compare the decay of the reflections more easily, the signals are normalised, $t = 0$ is defined when the amplitude of the signal is at its maximum, and a dB scale is used by taking “ $20 \cdot \log_{10}$ ” of the voltage amplitude (see Figure 17 and Figure 18).

Thus, we can notice that the choice of the termination in the simulations does affect the response, in particular when the analogue signal chain is used. The 35-m cables have a significant impact in this simulation, adding reflections up to -38 dB after 310 ns, and potentially contaminating $k_{||}$ -modes between 0.14 and 0.18 h/Mpc in this scenario. Note that for 100-m cables, these reflections would occur after 890 ns, so for $k_{||}$ -modes after 0.45 h/Mpc at 150 MHz. Depending on how the antenna is terminated, variations of up to 20 dB can be observed in the antenna voltage response. Therefore, a proper termination should be used to more accurately estimate the contamination of the EoR window.

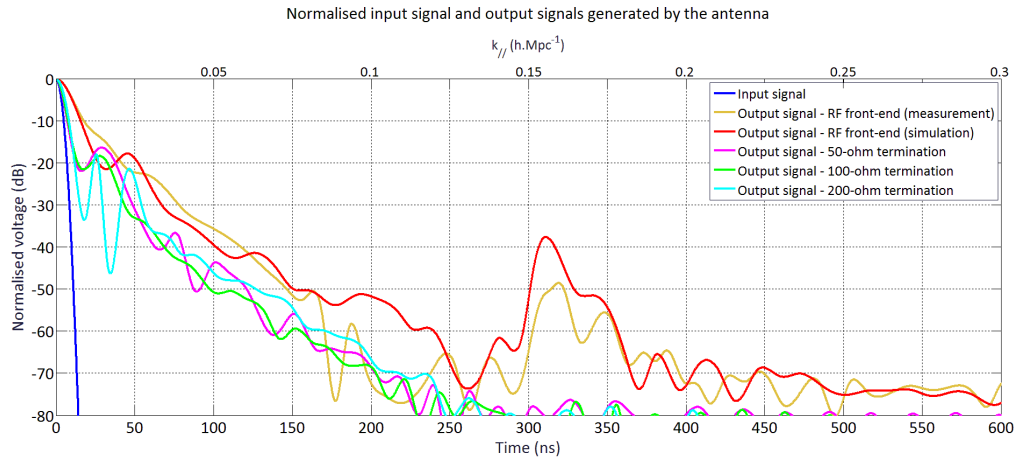


Figure 17. Normalised input (50 – 250 MHz) and output signals, when the antenna is terminated by a fix impedance (50, 100 and 200 Ω), and by the simulated and measured S-parameters of the front-end with a cable length of 35m. $t = 0$ is defined when the amplitude of the signal is maximum.

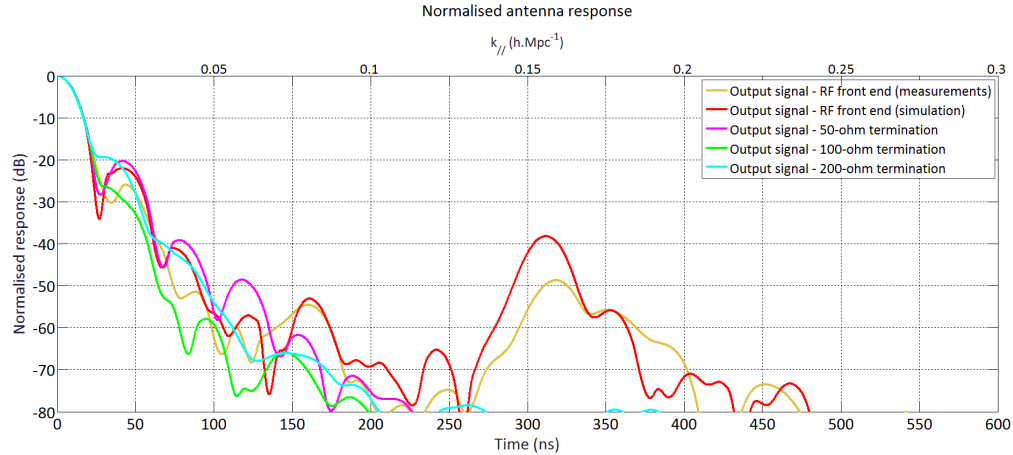


Figure 18. Voltage antenna response, for different terminations. A Blackman-Harris window function was applied to filter the frequency response between 100 and 200 MHz.

Lastly, it is interesting to compare *Figure 7* with *Figure 18*, and see that the results are coherent. Indeed, overall the antenna impedance is closer to 100 Ω than to 50 or 200 Ω , which explains why the level of reflections is lower in this case. In addition, the simulated RF front-end has an impedance rather close to 50 Ω , and consequently their voltage response is rather similar, in particular at low delay before the effects of the cable are visible. Note that this is less visible in *Figure 17*, since an input signal between 50 and 250 MHz was used, and that the antenna is “optimised” between 100 and 200 MHz. Still in *Figure 17*, we can also notice that the level of reflections in the output signal with the RF front-end is higher, compared to 50 or 100 Ω for example, even though its impedance varies smoothly between 50 and 100 Ω . This difference can be explained by the fact that the filter in the receiver acts as a square window function, in the frequency domain (see *Figure 19*). And as explained previously, such a window presents high sidelobes in the time domain, which spreads the signal and increases the level of reflections. Thus, this simulation allows us to account for this effect, and demonstrates the benefit of using an additional “sharp” windowing function.

3.2.2. Frequency response

The same analysis can be performed in the frequency domain for comparison. *Figure 19* shows the spectrum of the “50-250 MHz” input signal defined in CST, as well as the spectrum of the output signals after the balun and after the front-end (component models from simulation). Thus, we can see how the spectral structure of the incoming signal is modified by the antenna beam, the reflections, the gain of the front-end, and the filter. Note that the small ripples visible on the spectrum of the balun and the front-end are caused by the reflections in the cable. The spectrum of the transfer function, obtained after processing with the Blackman-Harris window between 100 and 200 MHz, is also presented.

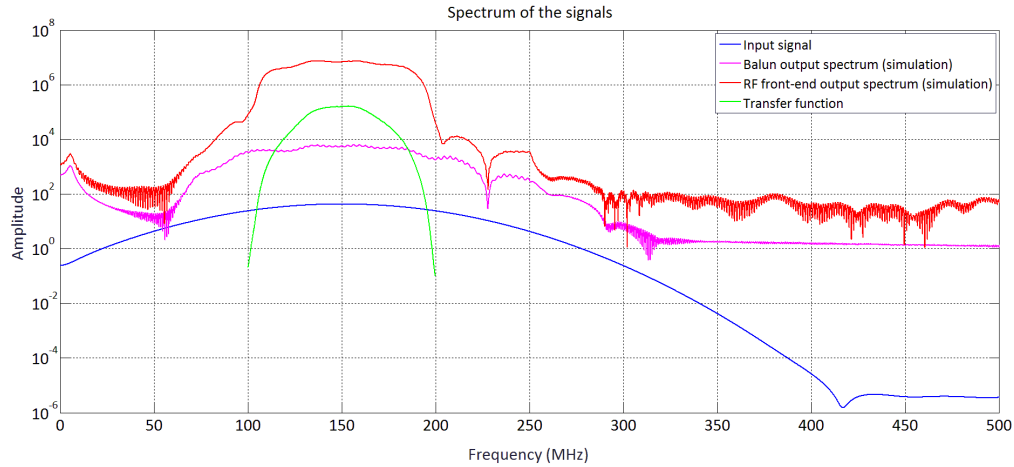


Figure 19. Spectrum of the “50-250 MHz” input signal, output signals after the balun and the front-end, and voltage transfer function (with Blackman-Harris window).

Lastly, Figure 20 below shows the effects of the termination impedance on the differential S_{dd} -parameter of the HERA dish. As expected, the level of the different S-parameters is coherent with what we observed with the time domain responses. For comparison, we also added the S-parameter of the PAPER feed terminated by the measured RF front-end parameters. Contrary to the HERA dish, its impedance does not vary a lot, and consequently it was possible to easily match it between 100 and 200 MHz, with a stable S_{dd} of about -8 dB.

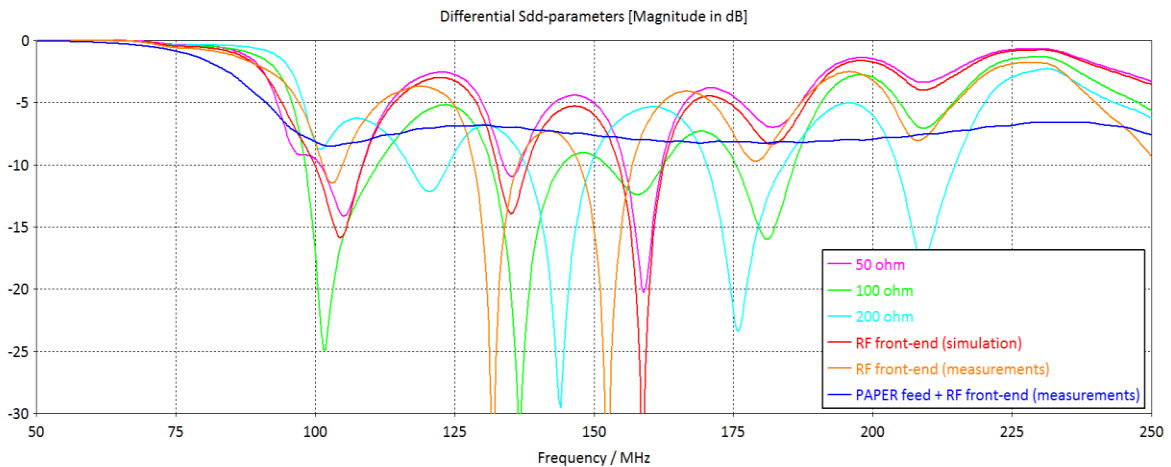


Figure 20. Differential S_{dd} -parameters of the HERA dish, for different terminations. For comparison, the S_{dd} of the PAPER feed terminated by the measured RF front-end is also plotted.

Conclusion

In this memo, we presented a method to accurately simulate the HERA analogue signal chain, and its effects on the received signal, in terms of reflection, gain, propagation, and noise. First, the S-parameters and noise figures of the active balun, RG6U cables, and receiver were simulated with Genesys, and then measured with a VNA. In particular, the front-end with a 100-m coaxial cable has a total gain of about 87.5 dB, and a 3dB-bandwidth of 76.5 MHz between 111 and 188 MHz due to its bandpass filter. Moreover, when connected to the proper antenna impedance, its noise temperature varies between 140 K and 215 K, except at low frequency below 105 MHz, and at high frequency above 195 MHz, where it rockets. This can be explained by two factors: the limited bandwidth of the filter, and the very high antenna impedance which causes a bad impedance matching for the noise with the front-end. Consequently, the antenna sensitivity at the zenith is not very good at low frequency ($\sim 0.1 \text{ m}^2/\text{K}$) and bad at high frequency ($\sim 0.05 \text{ m}^2/\text{K}$), which may be problematic to retrieve useful data from the noise.

Once the S-parameters of the front-end are generated, it is possible to combine them in a co-simulation with the electromagnetic model of the antenna by using CST. Thus, this method allows us to simulate the output signal generated by the antenna at any point of the RF chain, in the time and frequency domain, when the system is excited by a plane wave coming from the zenith. As we saw, the impedance termination of the antenna is a key parameter to characterise the reflections occurring at the interface between the antenna and the front-end. Besides, the antenna impedance varies a lot between 100 and 200 MHz, which makes the impedance matching complicated. The time simulation shows that the level of reflection level in the voltage antenna response windowed by a Blackman-Harris window falls below -60 dB after 175 ns, which corresponds to k_{\parallel} -modes above 0.09 h/Mpc. However, it also reveals that the cable can cause problematic reflections at its interfaces with the balun and the receiver. Indeed, as an example, for a 35-m RG6U cable reflections above -38 dB are visible after 310 ns, which corresponds to the round trip time of the signal in the cable. In this scenario, k_{\parallel} -modes up to 0.18 h/Mpc would be contaminated. Note that this is just a model, but we should be very careful if short coaxial cables are used.

Lastly, it will be interesting to use this method again to estimate the performances of the new Vivaldi or sinuous feed, combined with the new RF front-end under development.

References

1. Genesys RF and Microwave Design Software. Available at: <http://www.keysight.com/en/pc-1297125/genesys-rf-and-microwave-design-software?cc=GB&lc=eng>.
2. Fagnoni, N. & de Lera Acedo, E. An Updated Electromagnetic Simulation of the HERA Antenna with CST and Comparison with Measurements. (2017).
3. Ewall-Wice, A. *et al.* The Hydrogen Epoch of Reionization Array Dish II: Characterization of Spectral Structure with Electromagnetic Simulations and its science Implications. (2016).
4. Thyagarajan, N. *et al.* Effects of Antenna Beam Chromaticity on Redshifted 21 cm Power Spectrum and Implications for Hydrogen Epoch of Reionization Array. (2016).
5. Parashare, C. & Bradley, R. Instrument Development for PAPER: a Precision Array to Probe the Epoch of Reionization. (2011).
6. Parashare, C. & Bradley, R. 75 Ω Transmission System. (2011).
7. Parashare, C. & Bradley, R. 120-205 MHz Receiver for PAPER: Precision Array to Probe the Epoch of Reionization. (2011).
8. Analog Devices. Hittite HMC476MP86 Amplifier Spec. Available at: <http://www.analog.com/media/en/technical-documentation/data-sheets/hmc476mp86.pdf>.
9. CEL. NE461M02 NPN Transistor Spec. Available at: <http://www.cel.com/pdf/datasheets/ne461m02.pdf>.
10. Emhiser. TeleTec HX62 180° Hybrid Coupler Spec. Available at: <http://www.emhiser.com/images/datasheet/HX62A.PDF>.
11. KR Electronics. KR 2746 Bandpass Filter Spec. Available at: <http://krfilters.com/filter-docs/2746.pdf>.
12. Emhiser. TeleTech TX60 Transformer Spec. Available at: <http://www.emhiser.com/images/datasheet/TX60 SERIES.pdf>.
13. Anaren. Measurement Techniques for Baluns. (2015).
14. Maxim Integrated Product. Single-Ended and Differential S-Parameters. (2008)
15. Pozar, D. in *Microwave Engineering* (ed. Wiley) 191 – 211. (1998).
16. Abidi, A. & Leete, J. De-Embedding the Noise Figure of Differential Amplifiers. (1999).
17. Pozar, D. in *Microwave Engineering* (ed. Wiley) 628 – 632. (1998).
18. de Lera Acedo, E. *et al.* Ultra-Wideband Aperture Array Element Design for Low Frequency Radio Astronomy. (2011).
19. Medellin, G. Antenna Noise Temperature Calculation. (2007)
20. Furlanetto, S. The 21-cm Line as a Probe of Reionization. (2015).
21. Remazeilles, M. *et al.* An Improved Source-subtracted and Destriped 408 MHz All-sky Map. (2015).
22. Kolitsidas, C. & de Lera Acedo, E. Foreground Modeling and Antenna Calibration Errors for λ 21-cm Global Experiments. (2017).